

# Pairing, crystallization and string correlations of mass-imbalanced atomic mixtures in one-dimensional optical lattices

Tommaso Roscilde,<sup>1</sup> Cristian Degli Esposti Boschi,<sup>2</sup> and Marcello Dalmonte<sup>3</sup>

<sup>1</sup>*Laboratoire de Physique, CNRS UMR 5672, Ecole Normale Supérieure de Lyon, Université de Lyon, 46 Allée d'Italie, Lyon, F-69364, France*

<sup>2</sup>*CNR-IMM, Sezione di Bologna, via Gobetti 101, I-40129, Bologna, Italy*

<sup>3</sup>*Dipartimento di Fisica and INFN, Università di Bologna, via Irnerio 46, I-40126, Bologna, Italy*

(Dated: June 2, 2022)

We numerically determine the very rich phase diagram of mass-imbalanced binary mixtures of hardcore bosons (or equivalently – fermions, or hardcore-Bose/Fermi mixtures) loaded in one-dimensional optical lattices. Focusing on commensurate fillings away from half filling, we find a strong asymmetry between attractive and repulsive interactions. Attraction is found to always lead to pairing, associated with a spin gap, and to pair crystallization for very strong mass imbalance. In the repulsive case the two atomic components remain instead fully gapless over a large parameter range; only a very strong mass imbalance leads to the opening of a spin gap. The spin-gap phase is the precursor of a crystalline phase occurring for an even stronger mass imbalance. The fundamental asymmetry of the phase diagram is at odds with recent theoretical predictions, and can be tested directly via time-of-flight experiments on trapped cold atoms.

PACS numbers: 37.10.Jk, 05.30.Jp, 71.10.Pm, 03.75.Lm

arXiv:1105.1314v1 [cond-mat.str-el] 6 May 2011

One-dimensional quantum liquids occupy a special place in the context of quantum many-body systems: indeed interactions of any strength lead to quantum fluctuations as strong as to discard Bose condensation for bosons and the Fermi liquid picture for fermions down to zero temperature. For sufficiently weak interactions a new unifying paradigm of the so-called Tomonaga-Luttinger liquids (TLL) emerges [1], characterized by the fact that all elementary excitations are gapless, and both diagonal and off-diagonal correlations decay algebraically with the distance. Recent advances in the trapping of ultracold atoms in optical lattices allow to realize one-dimensional quantum liquids in a highly flexible way, with the possibility of fully controlling the statistics and the interaction strength [2]. A series of recent experiments has demonstrated the physics of one-dimensional Bose gases with strong interactions up to the hardcore (or Tonks-Girardeau) limit [3]. A special role in the context of one-dimensional systems is played by binary mixtures, either bosonic, fermionic, or Bose-Fermi ones, for which TLL theory predicts the separation of spin and charge modes [1]. In the case of particles with equal masses and repulsive short-range interactions, both charge and spin sectors can be gapless, and one recovers an effective picture of two decoupled TLLs. Such a picture can be made unstable via several mechanisms: via Mott localization in presence of an underlying lattice and for integer total filling; via localization into a true (long-range-ordered) crystal (TC) in presence of a strong off-site repulsion; via phase separation; or via the formation of bound states (*e.g.* Cooper pairs for attractive interactions) leading to the appearance of a spin gap.

Here we show that the TLL picture undergoes a complex series of instabilities in binary mixtures with *mass imbalance* between the two species. We focus here on quantum particles on a lattice with intraspecies hardcore repulsion and on-site interspecies interactions, describing at the same time spin-1/2

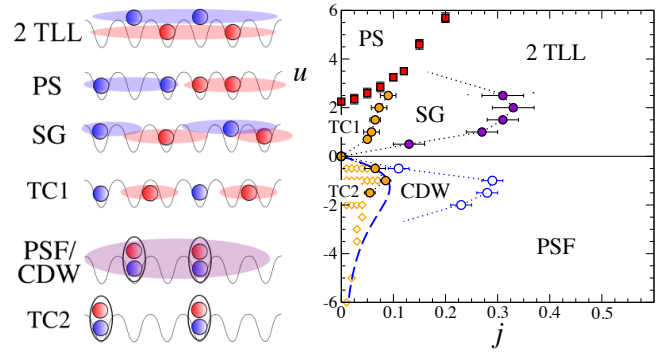


FIG. 1: Phase diagram of a mass-imbalanced atomic mixture with filling  $n_a = n_b = 1/3$ . The phase boundaries are determined via QMC; the open diamonds indicate points in parameter space for which DMRG finds a fully gapped crystal phase TC2. The dashed line indicate the FK gap  $\Delta_k/J_a$  for kink-antikink pairs. The left panel presents a sketch of the phases: 2 TLL = 2 Tomonaga-Luttinger liquids; PS = phase separated; SG = spin gap; PSF = pair superfluid; CDW = algebraic charge density wave; TC1 and TC2: true crystals.

fermions, spin-1/2 hardcore bosons, and mixtures of hardcore bosons and spinless fermions. The system Hamiltonian reads

$$\mathcal{H} = \sum_i \left[ -(J_a a_i^\dagger a_{i+1} + J_b b_i^\dagger b_{i+1} + \text{h.c.}) + U n_{i,a} n_{i,b} \right] \quad (1)$$

in which  $a$  and  $b$  correspond to the two atomic species. Mass imbalance is controlled by the ratio  $j = J_b/J_a$  and interaction by the ratio  $u = U/J_a$ . As far as the spectrum and the diagonal observables are concerned, we do not need to specify the statistics of the  $a$  and  $b$  operators; for what concerns off-diagonal observables, unless otherwise specified we will refer explicitly to hardcore bosons, satisfying bosonic commutation relations off-site and fermionic anticommutation relations on-site. The denomination of the many-body phases will also be mostly inspired by the case of hardcore-boson mixtures.

We consider both repulsive ( $u > 0$ ) and attractive ( $u < 0$ ) interactions, and we focus on the case of equal densities away from half filling,  $n_a = n_b = 1/p \neq 1/2$ ,  $p \in \mathbb{N}$ . The system with equal masses,  $j = 1$ , is integrable [4], and features spin-charge separation into two TLL in the repulsive case; in the attractive one, an  $a$ - $b$  bound state appears, associated with the opening of a spin gap, and only the charge sector remains gapless, giving rise to a paired superfluid (PSF) phase. The case of mass imbalance has been studied recently by bosonization [5–7], and numerically via the density-matrix renormalization group (DMRG) and related approaches [8–10].

Making use of numerically exact methods, here we determine comprehensively the rich phase diagram of the system with mass imbalance,  $j < 1$ , as shown in Fig. 1. The latter figure refers to the case  $n = 1/3$ , but the qualitative features are generic for commensurate fillings. Our main findings are the following: 1) in the attractive case, the PSF phase is found to persist up to strong imbalance, at which the system becomes unstable to the formation of a TC of pairs. 2) in the repulsive case, on the other hand, the double TLL of the mass-balanced case survives up to a large imbalance, at which two different instabilities appear. For sufficiently large repulsion, the two species phase-separate. For weaker repulsion, first a spin-gap opens, associated with fluctuating magnetic order captured by string correlations; this phase is the precursor of a TC phase with pinned  $b$  particles, and  $a$  particles localized in the interstitial regions.

Before discussing the derivation of the phase diagram, we point out that the physics described in this paper is largely accessible to current experimental setups on ultracold mixtures in one-dimensional optical lattices. The mass imbalance can be realized with heteronuclear mixtures (*e.g.*  $^{40}\text{K}$ - $^6\text{Li}$ , for the fermionic case,  $^{41}\text{K}$ - $^{87}\text{Rb}$  for the bosonic case, and  $^{40}\text{K}$ - $^{87}\text{Rb}$  for the Bose-Fermi case [11]), and with homonuclear mixtures in different hyperfine states, and it can be continuously tuned by using lasers with a wavelength close to the magic value or to an atomic resonance for one of the two species. The inter-species interaction can be tuned by Feshbach resonances, as widely demonstrated in the recent literature [11].

The phase diagram in Fig. 1 is the result of a joint numerical study based on quantum Monte Carlo (QMC) and DMRG[12]. Our QMC calculations are based on a canonical formulation [13] of the Stochastic Series Expansion approach with directed loops [14], applied to chains with up to  $L = 150$  sites with periodic boundary conditions, and at temperatures  $\beta J_b = L$  capturing the  $T = 0$  physics for both species. Our DMRG calculations apply to chains with up to  $L = 144$  with open boundary conditions and retaining up to  $M = 1400$  states.

We start our discussion by the attractive case. For a very broad range of mass imbalance, the system displays a PSF phase, characterized by quasi-condensation of bound  $a$ - $b$  pairs, giving rise to an algebraic decay of the pairing correlation function [1],  $G_{ab}(r) = \langle a_i^\dagger b_i^\dagger b_{i+r} a_{i+r} \rangle \sim r^{-1/K_\rho}$ ; density-density correlations are also decaying algebraically as  $C_\rho(r) = \langle n_i n_{i+r} \rangle - \langle n_i \rangle \langle n_{i+r} \rangle \approx -\frac{K_\rho}{\pi^2 r^2} + A \frac{\cos(2\pi n r)}{r^{K_\rho + K_\sigma}}$ ; here,

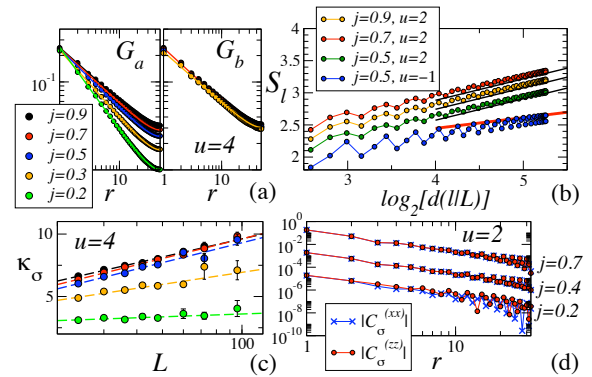


FIG. 2: Evidences for the absence of spin gap for moderate mass imbalance. (a) Green’s function for both species (solid lines are fits to  $A_{a(b)}d(r|L)^{-1/(2K_{a(b)})}$ ,  $L = 96$ ); (b)  $\kappa_\sigma$  coefficient (dashed lines are linear fits); all data are for  $u = 4$ ; (c) Block entropy  $S_l$  for chains with  $L = 120$  sites (the curves for  $j = 0.5$  and  $j = 0.7$  are shifted to improve readability); thick lines are a reference for  $c = 2$  (black) and  $c = 1$  conformal field theories (red); (d) Fermionic spin-spin correlation functions, calculated via DMRG between the sites  $L/3$  and  $2L/3$  of a chain with  $L = 96$ . The data for  $j = 0.4$  and  $j = 0.2$  have been rescaled to improve readability (by a factor  $10^{-2}$  and  $10^{-4}$ , respectively).

$n_i = n_{i,a} + n_{i,b}$ , and  $K_\rho$  is the charge TLL parameter. For equal masses,  $K_\rho > 1$  [1] for all  $u < 0$ , so that the dominant correlations are the pairing ones. Moreover  $K_\sigma = 0$  due to the presence of the spin gap (see below). We extract the Luttinger exponent from the slope of the density structure factor at  $q \rightarrow 0$ ,  $S_\rho(q) = \sum_r \exp(iqr) C_\rho(r) \approx K_\rho q/\pi$ , and we find that mass imbalance leads to a reduction of  $K_\rho$ , consistently with what observed for other fillings in Ref. [10]. For large mass imbalance,  $K_\rho$  becomes smaller than one: this corresponds to the loss of quasi-condensation, in favor of a quasi-solid phase (or charge density wave, CDW), with dominant density correlations. This phase is the precursor of a quantum phase transition to a TC of pairs – phase TC2 of Fig. 1 – with the onset of long-range density order at wavevector  $Q = 2\pi n$ . We determine the extent of the TC phase via QMC by determining the mass imbalance at which  $S_\rho(Q)$  starts diverging linearly with system size; and by DMRG detecting the onset of the exponential decrease of  $G_{ab}$  and  $C_\rho$ , marking the opening of a charge gap [15]. The TC instability is well understood coming from the Falicov-Kimball (FK) limit,  $J_b = 0$ . In this limit, which reduces to a 1D lattice gas in a static potential, we find that the ground state corresponds to the TC of pairs for all values  $u < 0$ . The gap  $\Delta_k$  to the formation of kink-antikink pairs in the TC is found to be a non-monotonic function of  $|u|$ , displaying an intermediate maximum. We observe that, for small  $|u|$ , the boundary of the crystalline region follows closely the locus at which the gap  $\Delta_k$  equals  $J_b$ , and it has a re-entrant shape mimicking the non-monotonic behavior of the gap as a function of  $u$ . This suggests that the quantum melting transition corresponds to a condensation of kink-antikink pairs in the ground state.

The repulsive side of the phase diagram is more complex. Combining bosonization with renormalization group

calculations up to two loops, Refs. 5, 6 conclude that a spin gap should open for any infinitesimal mass imbalance as  $\Delta_s \approx \Lambda \exp(-A'/|J_a - J_b|)$  for  $J_b \lesssim J_a$ , where  $\Lambda \sim J_a, J_b$ . On the contrary, Ref. 7, also based upon bosonization, concludes that the spin gap is absent in the repulsive case. All our numerical findings point toward the persistence of a fully gapless TLL behavior for both the charge *and* spin sector over a dominant portion of the repulsive phase diagram. Our conclusion is based on a number of crossed evidences. First of all, we observe that the one body correlation functions  $G_a(r) = \langle a_i^\dagger a_{i+r} \rangle$  and  $G_b(r) = \langle b_i^\dagger b_{i+r} \rangle$  can be very well fitted with the simple power-law form  $G_{a(b)}(r) = A_{a(b)} d(r|L)^{-1/(2K_{a(b)})}$ , where  $d(r|L) = L |\sin(\pi r/L)|/\pi$  is the conformal distance (see Fig. 2(a)). In particular we find that, for weak and moderate repulsions,  $K_{a(b)} > 0.5$ , which implies that the momentum distribution  $n_{a(b)}(q) = \sum_r \exp(iqr) G_{a(b)}(r)$  displays a quasi-condensation divergent peak at  $q = 0$ , to be detected in time-of-flight experiments (see below). Moreover we exploit the fact that an explicit counting of the number of gapless degrees of freedom in the system comes from the central charge  $c$  of the conformal field theory corresponding to our model of interest. This quantity can be directly extracted via DMRG, using the fundamental result that the entanglement entropy (EE) of a boundary block of the system grows with the size  $l$  of the block [16] as  $S_l = -\text{Tr}(\rho_l \log_2 \rho_l) \approx \frac{c}{6} \log_2[d(l|L)] + \mathcal{O}(1/l) + \text{const}$ , where  $\rho_l$  is the reduced density matrix of the boundary block, and open boundary conditions are employed. Fig. 2(b) (see also Ref. [15]) shows that the scaling of the EE is fully consistent with  $c = 2$  in the repulsive regime, providing further evidence for the fact that the TLL has two gapless components even for a significant mass imbalance.

Finally, using QMC we gain further insight into the gapless phase by investigating the spin-spin correlation function  $C_\sigma^{(zz)}(r) = \langle S_i^z S_{i+r}^z \rangle \approx -\frac{K_\sigma}{\pi^2 r^2} + B \frac{\cos(2\pi nr)}{r K_\sigma + K_\sigma}$ ; where  $S_i^z = (n_{i,a} - n_{i,b})$ , and  $K_\sigma$  is the spin TLL parameter; in absence of a spin gap,  $K_\sigma \geq 1$ . We extract the Luttinger exponent from the low- $q$  behavior of the spin structure factor,  $S_\sigma(q) \approx K_\sigma q/\pi$ , giving the finite-size estimate  $K_\sigma(L) = [(L/2)S_\sigma(2\pi/L; L) + (L/4)S_\sigma(4\pi/L; L)]/2$ . At the SU(2) invariant point  $j = 1$ ,  $K_\sigma(L)$  is known to obey the Kosterlitz-Thouless (KT) critical scaling  $K_\sigma(L) \approx 1 + [a \log(L/L_0)]^{-1}$  [1], which implies that the quantity  $\kappa_\sigma(L) = [K_\sigma(L) - 1]^{-1}$  scales linearly with  $\log(L)$ . Quite remarkably, this scaling law remains valid over a broad range of  $j < 1$  values, and even for strong inter-species coupling, as shown in Fig. 2(c). This means that, even if the SU(2) symmetry is broken in the Hamiltonian, it appears to be restored in the ground-state of the system, namely that a moderate mass imbalance is an *irrelevant* perturbation and that, under a renormalization group treatment, the system flows to the SU(2)-symmetric fixed point  $K_\sigma(L \rightarrow \infty) \rightarrow 1$  over a broad range of  $j$  values. This picture is further corroborated by comparing the longitudinal spin-spin correlations  $C_\sigma^{(zz)}(r)$  and the transverse ones in the *fermionic case*,  $C_\sigma^{(xx)}(r) = \langle S_i^x S_{i+r}^x \rangle$ , where

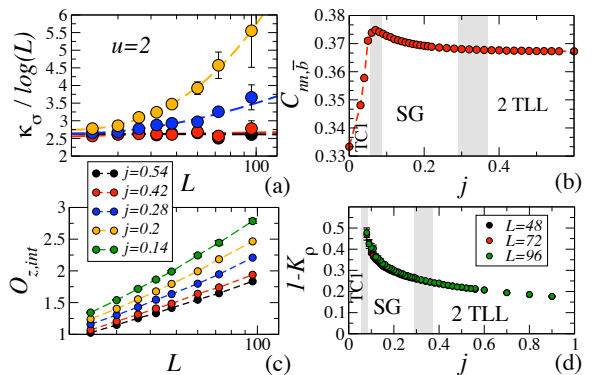


FIG. 3: (a) Breakdown of SU(2)-invariant scaling of  $\kappa_\sigma$  for  $u = 2$  and decreasing  $j$ ; dashed lines are fits to  $a_1/\log(L) + a_2 \log(L)^{\alpha_3}$ ; (b)  $b$ -hole density correlator for nearest neighbors,  $L = 30$ ; the shaded areas mark the transition regions among the various phases; (c) String structure factor as a function of system size (same parameters as in (a)); (d) Decay exponent of the string correlation function as function of  $j$ .

$S_i^x = a_i^\dagger b_i + b_i^\dagger a_i$ ; the two correlation functions show the same algebraic decay over a broad range of  $j$  values, and they even appear to coincide at short range, as shown in Fig. 2(d).

On the other hand, a careful study of the behavior of the system shows that the two-component TLL becomes indeed unstable to the formation of a spin gap (SG) for *strong* mass imbalance ( $j \lesssim 1/3$  for  $n = 1/3$ ). The opening of a spin gap leaves a clear signature in the Luttinger exponent  $K_\sigma$ , which stops flowing to the SU(2) symmetric value: this is seen in the fact that  $\kappa_\sigma$  begins to scale *faster* than linearly in  $\log(L)$ , which is a manifestation of the fact that  $K_\sigma(L)$  flows to values smaller than 1, as shown in Fig. 3(a). We use this criterion to locate the opening of the spin gap in Fig. 1. Moreover the breaking of SU(2) symmetric scaling is also seen in the spin-spin correlation functions, which acquire a different behavior at short and long distances (see Fig. 2(d)). The opening of a spin gap signals the formation of a bound state of some sort: but what could this bound state be in a purely repulsive system? We argue that a bound state can appear between the  $a$  particles and the *holes* of the  $b$  species, which are in a commensurate proportion  $m = (1 - n)/n$  to the  $a$  particles. As shown in Ref. 17, a sufficiently strong mass imbalance can indeed bind together particle composites in 1D quantum fluids - in the specific case of  $n = 1/3$  we have trimers formed by one  $a$  particle and two  $b$  holes ( $\bar{b}$ ). For strong enough repulsion ( $u \gtrsim 1$ ) the apparition of  $a$ - $2\bar{b}$  composites is seen in the nearest-neighbor density correlations of the  $\bar{b}$  holes,  $C_{n\bar{n},\bar{b}} = \langle (1 - n_{i,b})(1 - n_{i+1,b}) \rangle$ , which is enhanced for increasing mass-imbalance, as seen in Fig. 3(b).

The  $a$ - $2\bar{b}$  composites have mutual repulsive interactions, as observed in Ref. 18, so that their binding favors configurations of the type  $\dots a0ba0b0a0b0ab\dots$  in which the  $a$  and  $b$  particles alternate spatially. Such configurations, albeit lacking long-range density and magnetic order, contain strong non-local correlations that can be captured using a *string correlation function*[19]  $O_z(r) = -\langle S_i^z e^{i\pi \sum_{j=i+1}^{i+r-1} S_j^z} S_{i+r}^z \rangle$ . As

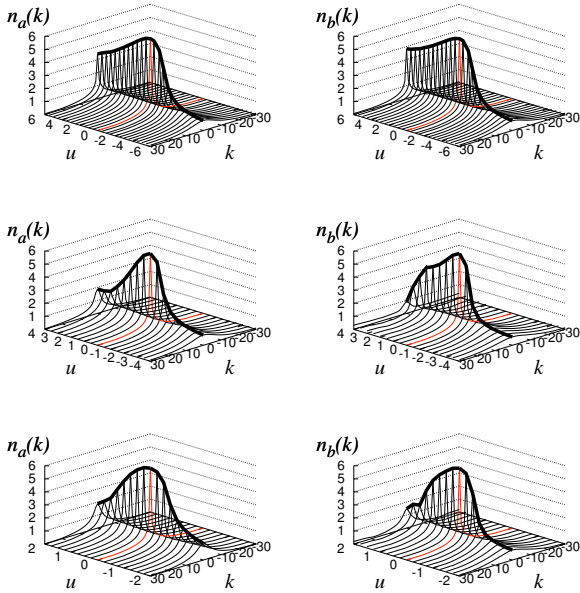


FIG. 4: Evolution of the momentum distribution of both species on a  $L = 60$  chain, for interactions spanning the repulsive and the attractive side at fixed mass imbalance. From top to bottom:  $j = 2/3, 1/10, 1/20$ .

shown in Fig. 3(c-d), string correlations are significantly enhanced when entering the SG phase: indeed the string structure factor,  $O_{z,int} = \sum_r O_z(r)$ , shows a more pronounced divergence with system size, which signals the slower decay of  $O_z(r)$ . As shown in Ref. 15, in presence of spin-charge separation the dominant decay of the string correlations is governed solely by the  $K_\rho$  exponent,  $O_z(r) \sim r^{-K_\rho}$ ; therefore  $K_\rho$  controls the divergence of  $O_{z,int} \sim L^{1-K_\rho}$ , and in Fig. 3(d) we observe that the  $1 - K_\rho$  exponent (extracted from the low- $q$  behavior of  $S_\rho(q)$ ) is significantly enhanced in the SG phase. Given that both the spin and charge structure factor exhibit a peak whose divergence with system size is hindered by the slow size-scaling of the divergence exponent  $1 - K_s - K_\rho$  [15], we find that the string correlations best characterize the “fluid” magnetic order of the SG phase.

The bound trimers appearing in the SG phase undergo crystallization - phase TC1 in Fig. 1 - for moderate repulsion and extreme mass imbalance. The TC1 phase is analogous to the one discussed in Ref. 18 (see also Ref. 15). This phase is marked by a suppression of  $C_{nn,\bar{b}}$  which attains its absolute minimum  $C_{nn,\bar{b}} = 1 - 2n$  for  $j \rightarrow 0$ , due to the suppression of the weight of configurations with contiguous trimers. The resulting non-monotonic behavior of  $C_{nn,\bar{b}}$  as a function of  $j$ , shown in Fig. 3(b) (see also Ref. [15]), provides further evidence that the SG phase is a liquid of pre-formed trimers - the enhancement of  $C_{nn,\bar{b}}$  in that phase is due to trimer binding, while the suppression in the TC1 phase is due to crystal ordering of the trimers.

Our theoretical results have immediate consequences for current experiments on one-dimensional mixtures of mass-

imbalanced cold atoms. Such experiments can probe both attractive and repulsive interactions, within the same experimental conditions, via the use of Feshbach resonances [11]. Our phase diagram reveals a fundamental asymmetry between the attractive and the repulsive case for weak and moderate mass imbalance, with the formation of bound pairs on the attractive side and the absence of spin gap on the repulsive one. This asymmetry is very well seen in time of flight experiments probing the momentum distributions  $n_a(k)$ ,  $n_b(k)$ , which are very broad on the attractive side, while they exhibit sharp quasi-condensation peaks on the repulsive side - as shown in Fig. 4. This asymmetry can be used as strong evidence of pairing on the attractive side. A partial symmetry is recovered only for strong mass imbalance, with the opening of a spin gap in the repulsive case, and the occurrence of a crystalline phase for both signs of the interaction. This is also well captured by the momentum distributions, showing this time a suppression of the quasi-condensation peaks on the repulsive side due to the appearance of the SG phase and of the crystalline phase. Finally the availability of high-resolution *in-situ* imaging [20] sensitive to the spin [21] allows to detect the formation of bound trimers and the enhancement of string correlations characterizing the SG phase.

We thank P. Azaria, S. Capponi, T. Giamarchi, F. Heidrich-Meisner, and E. Orignac for fruitful discussions, F. Ortolani for help with the DMRG code, and the PSMN (ENS-Lyon) for generous computer support. CDEB is grateful to CNISM Unit of the Physics Department, University of Bologna, where this work was started.

- 
- [1] T. Giamarchi, *Quantum Physics in One Dimension*, Clarendon Press, Oxford (2004).
  - [2] I. Bloch *et al.*, Rev. Mod. Phys. **80**, 885 (2008).
  - [3] T. Kinoshita *et al.*, Science **305**, 1125 (2004); B. Paredes *et al.*, Nature **429**, 277 (2004); E. Haller *et al.*, *ibid.* **466**, 597 (2010).
  - [4] F. H. L. Essler, H. Frahm, F. Göhmann, A. Klümper, and V. E. Korepin, *The One-Dimensional Hubbard Model*, Cambridge, 2005.
  - [5] M. A. Cazalilla *et al.*, Phys. Rev. Lett. **95**, 226402 (2005).
  - [6] L. Mathey, Phys. Rev. B **75**, 144510 (2007).
  - [7] Z. G. Wang *et al.*, Phys. Rev. B **75**, 165111 (2007).
  - [8] M. Rizzi and A. Imambekov, Phys. Rev. A **77**, 023621 (2008).
  - [9] B. Wang *et al.*, Phys. Rev. A **79**, 051604(R) (2009).
  - [10] L. Barbiero *et al.*, Phys. Rev. B **81**, 224512 (2010).
  - [11] C. Chin *et al.*, Rev. Mod. Phys. **82**, 1225 (2010), and references therein.
  - [12] S.R.White, Phys. Rev. Lett. **69**, 2863 (1992).
  - [13] T. Roscilde, Phys. Rev. A **77**, 063605 (2008).
  - [14] O. F. Syljuåsen, Phys. Rev. E **67**, 046701 (2003).
  - [15] See Supplementary Material.
  - [16] P. Calabrese and J. Cardy, JSTAT P06002 (2004).
  - [17] E. Burovski *et al.*, Phys. Rev. Lett. **103**, 215301 (2009).
  - [18] T. Keilmann *et al.*, Phys. Rev. Lett. **102**, 255304 (2009).
  - [19] M. den Nijs and K. Rommelse, Phys. Rev. B **40** 4709 (1989).
  - [20] W. S. Bakr *et al.*, Nature **462**, 74 (2009).
  - [21] C. Weitenberg *et al.*, Nature **471**, 319 (2011).

SUPPLEMENTARY MATERIAL

Attractive case: PSF-CDW and CDW-crystal transition

In this section we focus on the attractive case  $u < 0$ . The transition from the PSF phase to the CDW phase, obtained for decreasing hopping ratio  $j$ , is characterized by an inversion of the hierarchy between the pairing correlations,  $G_{ab}(r) \sim r^{-1/K_\rho}$ , and the density-density correlations  $C_\rho(r) \sim \cos(2\pi nr) r^{-K_\rho}$ . In the PSF phase  $K_\rho > 1$ , while in the CDW phase  $K_\rho < 1$ . The  $K_\rho$  exponent, extracted from the low- $q$  behavior of the density structure factor as discussed in the text, is shown in Fig. 5 as a function of  $j$  for various system sizes. A finite-size extrapolation allows to identify the critical  $j$  value at which  $K_\rho$  traverses the critical value  $K_\rho = 1$ . The composite  $a$ - $b$  pairs form therefore a TLL with effective exponent  $K_{\text{eff}} = K_\rho/2$ . In the CDW phase, we obtain a TLL with  $K_{\text{eff}} < 1/2$ , which is quite remarkable in a system with on-site interactions only. Indeed in one-component TLLs such a situation is realized only in presence of non-local interactions, such as nearest-neighbor or dipolar ones (R. Citro *et al.*, New J. Phys. 10, 045011 (2008); T. Roscilde and M. Boninsegni, New J. Phys. 12, 033032 (2010); M. Dalmonte *et al.*, Phys Rev Lett. 105, 140401 (2010)) or when considering highly-excited states such as a super-Tonks-Girardeau gas (G. E. Astrakharchik *et al.*, Phys. Rev. Lett. 95, 190407 (2005)). In our case, although the interactions between the  $a$  and  $b$  particles are on-site only, the bound  $a$ - $b$  pairs have effective longer-range interactions, decaying exponentially with the distance.

These effective interactions are responsible for the transition to crystalline order (phase TC2) at extreme mass imbalance. This transition occurs at the critical value  $K_{\text{eff}}^{(c)} = 2/p^2$ , where  $p = 1/n \in \mathbb{N}[1]$ . Since in our case  $p = 3$ , one obtains  $K_\rho^{(c)} = 4/9$  at the transition line, and  $K_\rho = 0$  in the crystalline phase, marking the onset of long-range density-density correlations. This implies the appearance of a peak diverging linearly in  $L$  at wavevector  $Q = 2\pi n$  in the structure factor for the total density  $S_\rho(q)$ , or alternatively in the density structure factor of both species

$$S_{a(b)}(q) = \sum_r e^{iqr} [\langle n_{i,a(b)} n_{i+r,a(b)} \rangle - \langle n_{i,a(b)} \rangle \langle n_{i+r,a(b)} \rangle]. \quad (2)$$

The onset of a linear-in- $L$  divergence of the structure factor peak is shown in Fig. 6, where the peak value divided by  $L$  is seen to converge to a finite value in the thermodynamic limit. This criterion has been used to determine the phase boundary between TC2 and CDW in Fig. 1.

A further clear signature of the TC2 phase is the exponential suppression of the pairing correlator  $G_{ab}$ , in sharp contrast with the algebraic decay of both CDW and PSF phases. We have used DMRG calculations with up to  $L = 144$  sites for fermionic  $a$  and  $b$  species in order to determine the extent of the TC2 phase (diamonds in Fig. 1). A typical set of data for

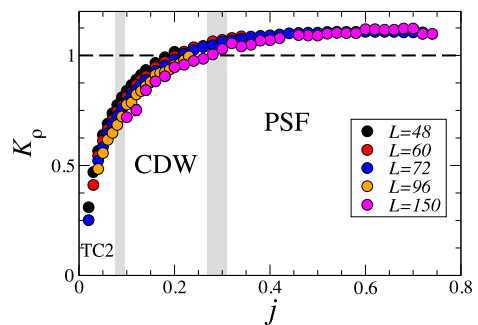


FIG. 5: Luttinger exponent  $K_\rho$  as a function of mass imbalance for the attractive case  $u = -1$  and  $n = 1/3$ . The shaded areas mark the estimated transition regions between the various phases.

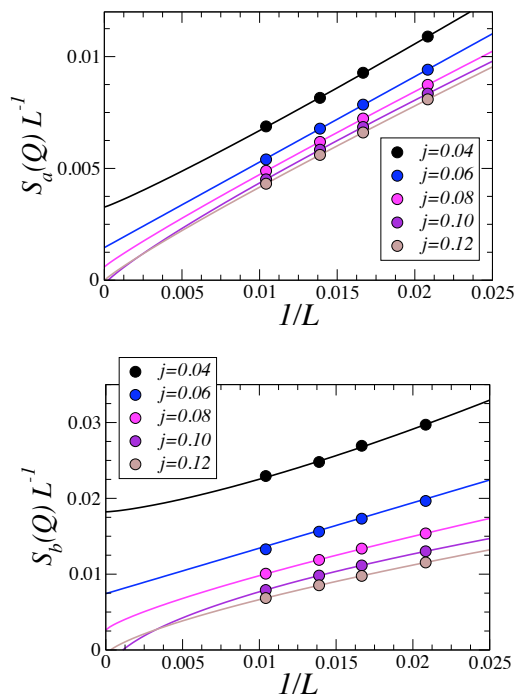


FIG. 6: Density structure factor for  $a$  and  $b$  particles at  $u = -1$  and various  $j$  values. Solid lines are fits to the form  $a_1 + a_2/L^{\alpha_3}$ .

$j = 0.03$  is presented in Fig. 7: there it is seen that for  $u = -1$  and  $-2$  the correlator  $G_{ab}$  decays exponentially; interestingly, for *stronger* attraction, *i.e.* for more tightly bound pairs, the correlation function acquires again an algebraic decay, showing the re-entrant nature of the TC2 phase. We observe that, close to the onset of the TC2, the decay of the  $G_{ab}$  correlator is indeed consistent with an exponent  $K_\rho^{(c)} = 4/9$ .

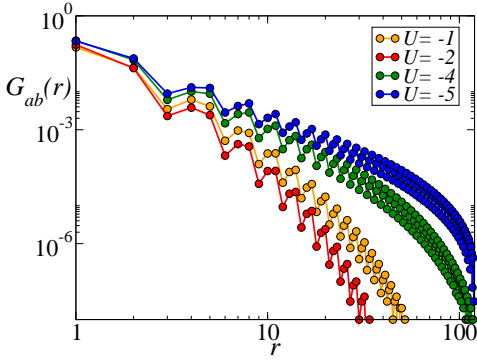


FIG. 7: Pairing correlation function on a  $L = 144$  system starting from  $L/6$  for  $j = 0.03$  and different interaction strength.

### Repulsive case: entanglement entropy analysis

As mentioned in the main text, the entanglement entropy (EE) allows to extract the central charge of the system[16]. In Fig. 8, we consider two different approaches to extract  $c$ . In the left panel, we plot  $S(l)$  as a function of the block length  $l$  at a fixed hopping asymmetry  $j = 0.5$  and fixed length  $L$ , for different values of  $u$ ; in the repulsive case, the numerical results are compatible with a completely gapless system, whereas in the attractive case the emergence of the spin gap reduces the central charge to 1. In the right panel, we plot the EE of the half chain

$$S(L/2) = \frac{c}{6} \log_2(L/\pi) + \mathcal{O}(1/L) + \text{const.} \quad (3)$$

which, for  $L = 6m, m \in \mathbb{N}$ , does not exhibit any oscillatory correction. For  $u > 0$ , all datas fit very well with the CFT prediction with  $c \simeq 2$ , whereas a clear bending at large system sizes indicates that a gap opens in the attractive case.

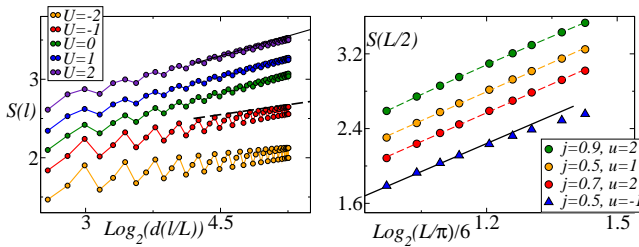


FIG. 8: Entanglement entropy of a subblock of length  $l$ . Left panel: EE scaling for  $L = 120, j = 0.5$  and different values of  $u$ ; for  $u \geq 0$  and  $u < 0$ , results are compatible with  $c = 2$  (black thick line) and  $c = 1$  (dashed line) respectively. Right panel: scaling of EE for  $l = L/2$  at different system sizes. In the repulsive case, datas are compatible with  $c = 2$ , whereas in the attractive one datas for larger system deviates toward  $c = 1$  at large  $L$ ; dashed lines are linear fits with  $c = 2.01, 2.07, 2.05$  from top to bottom, whereas the black, thick line represents  $c = 2$ . Data points for  $(j = 0.5, u = 1)$  and  $(j = 0.9, u = 2)$  have been shifted by 0.2, 0.5 to improve readability.

### Repulsive case: nearest-neighbor density correlations

Fig. 9 shows the nearest-neighbor correlation function for  $b$  holes,  $C_{nn,\bar{b}} = \langle (1 - n_{i,b})(1 - n_{i+1,b}) \rangle$  in the repulsive case. The calculation is performed via exact diagonalization on a chain with  $L = 12$  sites, which allows to access properly the true ground state in the limit  $j \rightarrow 0$ , both in the case of crystalline order and of phase separation. The latter limit is hard to reproduce appropriately with QMC or DMRG simulations, due to the abundance of metastable states close in energy to the ground state. We see that  $C_{nn,\bar{b}}$  is very sensitive to the succession of phases traversed by the system. As explained in the text, for small  $u$  values  $C_{nn,\bar{b}}$  is suppressed as  $j \rightarrow 0$  due to the formation of the crystal of  $a - 2\bar{b}$  trimers, implying that  $C_{nn,\bar{b}}$  has to attain its minimum value  $1 - 2n = 1/3$ . As  $j$  is reduced, two competing effects result in a non-trivial evolution of  $C_{nn,\bar{b}}$ . The formation of  $a - 2\bar{b}$  trimers leads to an enhancement of the  $C_{nn,\bar{b}}$  correlator: the kinetic repulsion between the  $\bar{b}$  holes, which would be normally present in a 1D single-component gas with hardcore repulsion, is strongly suppressed due to the decrease of the hopping ratio  $j$ , and therefore it is overcome by the binding effect of the light  $a$  particles, which gain energy by delocalizing over two (or more)  $\bar{b}$  holes. Yet the trimers that form via this mechanism experience an effective mutual repulsion at sufficiently small  $u$  values, due to the kinetic repulsion between light  $a$  particles. This leads to the suppression of configurations with adjacent trimers; a complete suppression of such configurations would lead the system to the trimer crystal state, which, as mentioned before and in the text, corresponds to an absolute minimum of  $C_{nn,\bar{b}}$ . Given that trimers are only loosely bound for small  $u$ , the effect of the repulsion between trimers dominates over the effect of trimer formation, so that  $C_{nn,\bar{b}}$  is seen to decrease monotonically for decreasing  $j$  ( $u = 1$  data in Fig. 9). On the other hand, for larger  $u$ , the enhancement of  $C_{nn,\bar{b}}$  due to trimer formation dominates over the suppression due to trimer repulsion, so that  $C_{nn,\bar{b}}$  is seen to increase for decreasing  $j$  down to the transition point to the crystalline phase, at which it drops down to the  $j \rightarrow 0$  limit ( $u = 2$  data in Fig. 9).

On the other hand, for even larger  $u$  the effective attraction between  $\bar{b}$  holes mediated by the  $a$  particles begins to involve more than two holes at once, as the  $a$ - $b$  interaction overcomes progressively the kinetic repulsion between  $a$  particles and favors their aggregation over extended clusters of holes. This phenomenon culminates into the phase separation between hole-rich and hole-free regions[10, 18] upon decreasing  $j$ , namely upon suppression of the kinetic repulsion between holes. This succession of phenomena leads to a much stronger enhancement of  $C_{nn,\bar{b}}$  as  $j$  decreases, with a steep increase when phase separation is achieved. When full phase separation is realized in the limit  $j \rightarrow 0$ ,  $C_{nn,\bar{b}}$  takes the value  $[(1 - n)L - 1]/L$  (namely  $7/12 = 0.583333$  for  $L = 12$ , as seen in Fig. 9).

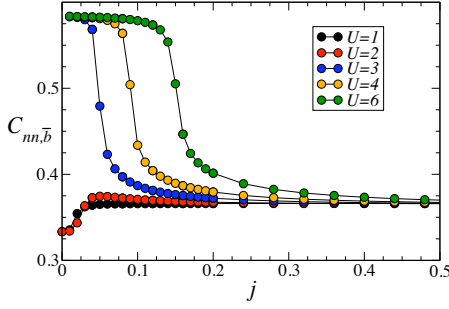


FIG. 9: Nearest-neighbor correlation function for  $b$  holes ( $\bar{b}$ ) for a chain or  $L = 12$  sites.

### Decay of string correlations from bosonization

In the following, we will study the dependence on the TLL parameters of the generalized string correlation function:

$$\mathcal{O}_\beta^z(r) = \left\langle \tilde{S}_i^z \exp \left[ i\pi\beta \sum_{i < k < i+r} \tilde{S}_k^z \right] \tilde{S}_{i+r}^z \right\rangle \quad (4)$$

where we have defined  $\tilde{S}_i^z = \frac{n_{a,i} - n_{b,i}}{2}$ . After applying standard bosonization identities to  $a, b$  operators by introducing the bosonic  $\phi_a, \phi_b$  fields[1], one can define *effective* spin and charge fields as  $\phi_{\sigma,\rho} = (\phi_a \mp \phi_b)/\sqrt{2}$  such that:

$$\tilde{S}_r^z = \frac{\partial_r \phi_\sigma(r)}{\sqrt{\pi}} + \gamma V_\rho^{\pm\sqrt{4\pi}}(r) V_\sigma^{\pm\sqrt{4\pi}}(r) + \dots \quad (5)$$

where  $V_{\sigma,\rho}^{\pm\alpha}(r) = e^{\pm i\alpha\phi_{\sigma,\rho}(r)}$  are vertex operators related to the charge and spin fields and  $\gamma$  is a constant; additional contributions with higher scaling dimension play no significant role in the remaining, and can thus be neglected. The non-local contribution in Eq. 4 can be reduced to:

$$\begin{aligned} \exp[i\pi\beta \sum_{i < k < i+r} \tilde{S}_k^z] &= \exp[i\pi\beta \int_i^{i+r} dy \frac{\partial_y \phi_\sigma(y)}{\sqrt{\pi}}] = \\ &= \exp[i\sqrt{\pi}\beta[\phi_\sigma(i+r) - \phi_\sigma(i)]] \end{aligned}$$

In addition to a pure spin contribution which stems from the first term in Eq. (5), and which decays faster than  $r^{-2}$ , the string correlator contains a more complicated, second contribution, stemming from vertex operators, and which we will indicate as  $\mathcal{O}_\beta^{z,2}$ . Assuming spin-charge separation,  $\mathcal{O}_\beta^{z,2}$  can be written as:

$$\begin{aligned} \mathcal{O}_\beta^{z,2}(r) &\propto \langle V_\rho^{+\sqrt{4\pi}}(i) V_\rho^{-\sqrt{4\pi}}(i+r) \rangle \times \\ &\times \langle V_\sigma^{\pm\sqrt{4\pi}}(i) V_\sigma^{-\beta\sqrt{\pi}}(i) V_\sigma^{\beta\sqrt{\pi}}(i+r) V_\sigma^{\mp\sqrt{4\pi}}(i+r) \rangle \\ &= \mathcal{M}_\sigma^{(\beta)}(r) * (1/r^{K_\rho}). \end{aligned}$$

whose asymptotic decay is affected by both charge and spin contributions: the charge part has a fixed exponent, whereas the spin one  $\mathcal{M}_\sigma^{(\beta)}(r)$  has a  $\beta$ -dependent form; in particular,

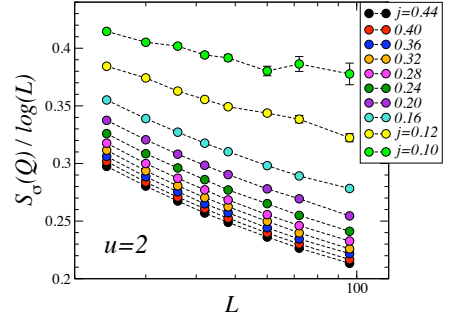


FIG. 10: Scaling of the peak in the spin structure factor for the repulsive case,  $u = 2$ .

for  $\beta = 2$  correlation considered in this work, the slowest decaying part of  $\mathcal{M}_\sigma^{(\beta)}(r)$  is a constant, so that the dominant term in the string correlation functions decays as:

$$\mathcal{O}_2^z(r) \propto 1/r^{K_\rho} \quad (6)$$

It is worth noticing that, from Eq. (6), one can easily recover standard spin correlations for  $\beta = 0$  decaying as  $1/r^{K_\rho + K_\sigma}$ .

The fact that the decay of string correlations is uniquely governed by the  $K_\rho$  exponent is indeed remarkable; as discussed in the main text, this leads to a string structure factor diverging with system size as  $O_{z,int} \sim L^{1-K_\rho}$  (and  $K_\rho < 1$  for all  $j$  values). This result has to be compared with the scaling of the peaks of the charge and spin structure factor, namely for  $S_\rho(Q)$  and  $S_\sigma(Q)$  with  $Q = 2\pi n$ . These peaks come from the dominant oscillating term (going like  $\cos(Qr)$ ) of the  $C_\rho(r)$  and  $C_\sigma(r)$  correlation functions, whose amplitude decays like  $r^{-K_\rho - K_\sigma}$ . This means that in general the  $Q$ -peak height scales with system size as  $L^{1-K_\rho - K_\sigma}$ . In the SG phase the  $K_\sigma$  exponent vanishes for  $L \rightarrow \infty$ , so that, strictly speaking, the true asymptotic scaling of  $S_\rho(Q)$  and  $S_\sigma(Q)$  is indeed the same as that of  $O_{z,int}$ . But *in practice* the scaling of  $K_\sigma(L)$  to zero is extremely slow – typically logarithmic, a fact which generates a huge finite-size correction to the effective scaling of  $S_\rho(Q)$  and  $S_\sigma(Q)$ . In our simulations we observe that these quantities grow more slowly than  $\log(L)$  over the entire SG phase for all the system sizes we considered (up to  $L = 96$  – see Fig. 10). To see them diverge at all with system size one might need exceedingly big system sizes, both for simulations and for experiments. Therefore string correlations stand as a unique tool to characterize the correlations in the SG phase.

### Repulsive case: onset of the crystalline phase

In this section we provide further details of the estimate of the transition line between the SG and the TC1 phase in the repulsive case. The transition is obtained by a joint finite-size

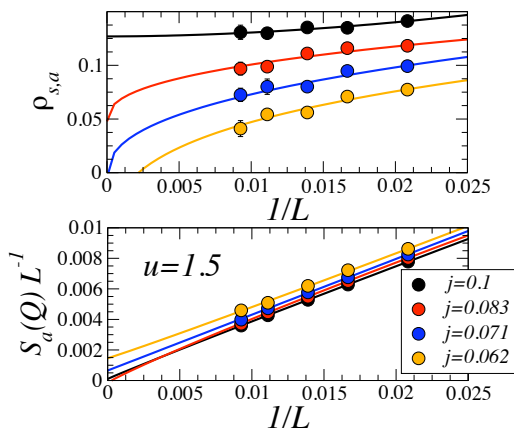


FIG. 11: Upper panel: scaling of the superfluid density of the  $a$  particles for  $u = 1.5$ . Lower panel: scaling of the peak in the density structure factor for the  $a$  particles. All solid lines are fits to the form  $a_1 + a_2/L^{a_3}$ .

scaling analysis. We focus on the scaling of the peak in the structure factors  $S_{a(b)}(q)$  appearing at  $Q = 2\pi n$ , and diverging linearly with system size when entering the TC1 phase; and we consider as well the scaling of the superfluid density for both species,  $\rho_{s,a(b)}$ , which scales to zero in the thermodynamic limit when in the TC1 phase. Fig. 11 shows that

the scaling of both quantities give a consistent estimate of the critical  $j_c$  value for the onset of crystalline order.

The transition to the TC1 phase was already estimated by one of the authors in Ref. [18] for the same density. The estimate of the transition line we present here is corrected with respect to that given in Ref. [18]. Indeed in Ref. [18] the estimate of  $j_c$  was biased by the choice of a scaling ansatz on the superfluid stiffness which, albeit satisfactorily verified within the statistical uncertainties, turns out to not be fully justified. The current estimate is not based on any scaling ansatz, and it delivers a transition line which is shifted to larger  $j_c$  values (typically by about 10-20 %) with respect to the estimates in Ref. [18].

Moreover Ref. [18] identified a narrow region of parameters close to the transition line as a *super-Tonks* regime, characterized by a sub-linearly diverging peak in the density structure factor of both species. The subtle effect of the opening of a spin gap before entering the crystalline phase was not observed in Ref. [18], and this led to the erroneous claim of algebraic off-diagonal correlations for both species in the super-Tonks regime. Our current results point to the fact that the above regime is rather characterized by superfluidity of both atomic species (which persists up to the transition, as shown in Fig. 11) but with exponentially decaying off-diagonal correlations, due to the presence of a spin gap.